Received: 22 December 2021 | Revised: 30 April 2022 | Accepted: 11 August 2022

DOI: 10.1002/asl.1129

RESEARCH ARTICLE

Atmospheric Science Letters RMetS

Upper-level midlatitude troughs in boreal winter have an amplified low-latitude linkage over Africa

Neil Ward[1] | **Andreas H. Fink**[2] | **Richard J. Keane**[1,3] | **Douglas J. Parker**[1,4,5]

[1]School of Earth and Environment, University of Leeds, Leeds, UK

[2]Institute of Meteorology and Climate Research, Karlsruhe Institute for Technology, Karlsruhe, Germany

[3]Met Office, Exeter, UK

[4]National Centre for Atmospheric Science (NCAS), University of Leeds, Leeds, UK

[5]NORCE Norwegian Research Center, Bjerknes Center for Climate Research, Bergen, Norway

Correspondence
Neil Ward, School of Earth and Environment, University of Leeds, Leeds LS2 9JT, UK.
Email: wardn626@gmail.com

Funding information
Transregional Collaborative Research Center SFB/TRR, German Research Foundation (DFG); AMMA-2050, Grant/Award Number: NERC/DFID_NE/M020126/1; Global Challenges Research Fund, African SWIFT program, Grant/Award Number: NE/P021077/1; IMPALA, Grant/Award Number: NERC/DFID NE/M017176/1; CEMAC, University of Leeds

Abstract

In boreal winter, strong upper-level midlatitude troughs across the Atlantic–Africa–southwestern Asia sector generate substantial tropical–extratropical interaction and have become recognized as important factors in some extreme weather events. As such, they represent important dynamic features to understand and capture in weather forecasts, as well as in climate models for projections on longer timescales. Here, we empirically study the 20% of winter days with strongest trough signatures during 1982–2020 at each longitude across the sector, and show that the trough impact over northern Africa, most notably in central parts, is particularly strong in magnitude, low-latitude extent and persistence, leading to the characterization of a northern Africa mode of several-days weather fluctuation. Weather conditions that follow strong troughs from the eastern Atlantic to the Central Mediterranean include: (i) a warming tendency across much of northern Africa, generally of several Celsius magnitude ahead of the trough, and >1°C even extending to the south of 10° N in central parts and continuing eastward until the Ethiopian Highlands; (ii) precipitation development further north than normal across northern tropical Africa, especially strong over longitudes corresponding to a northward extension of the main Congo rain belt. The intertropical discontinuity and low-level heat low are also shifted significantly north, with the complex of anomalies persisting for several days, beyond the timescale of the trough. For context, at all other trough longitudes across the sector, a warming signal does emerge (statistically significant), but with much shorter persistence (2–3 days), smaller magnitude and extending southward clearly only to 15–20° N. Mid-level tropical plumes of moisture are also typically present for strong troughs from the eastern Atlantic to southwestern Asia, and these alone can lead to weather extremes. However, low-level warming and mid-level moistening are uniquely juxtaposed at low latitudes over central Africa, where a near-equatorial signature develops.

KEYWORDS
Africa, Rossby waves, synoptic weather, temperature, tropical plume, troughs

1 | INTRODUCTION

The variability of low-level winter temperature across the Sahara has received relatively limited attention, yet is important to understand and predict from a climate modelling perspective (e.g., Cook & Vizy, 2015) as well as in the context of impactful heat waves in the region (Hu et al., 2019). Furthermore, it is known that wintertime northward migration of the intertropical discontinuity (ITD) in West Africa drawing unseasonable rains north of their typical latitude can trigger flooding rainfall events in the otherwise mostly arid setting at this time of year (Nicholson, 1981), with previous work showing that such fluctuations involved at least some warming to the north and often covaried with upper-level winter troughs over the eastern Atlantic approaching the western Mediterranean (e.g., Knippertz & Fink, 2008). Recently, upper-level winter troughs located near Iberia and the Central Mediterranean (CM) were shown to be followed by several days of particularly strong low-level warming across the Sahara including much of northeastern Africa, extending south of 10° N (Ward et al., 2021; Taylor et al., 2018; hereafter W21 and T18). Tropical moisture north of the equator was also impacted, with enhancement at low- and mid-levels, and a northward extension of the main Congo rain belt. These results built on previous work that showed midlatitude linkage into the tropics at this time of year over these or nearby longitudes (Bekele-Biratu et al., 2018; Camberlin & Philippon, 2002; Vizy & Cook, 2014). Further east over the Levant and Arabian Peninsula, midlatitude winter troughs have also been linked to anomalous moisture and precipitation to the south (De Vries et al., 2016; Ziv, 2001). A role is proposed for low- to mid-level moisture plumes extending from the deep tropics northeastward ahead of the trough (e.g., Fröhlich et al., 2013; Knippertz & Martin, 2005; Ziv, 2001). The linkage with low-level temperature was hypothesized in W21 and T18 to represent a further factor over northern Africa (i.e., Africa north of the equator) and particularly contributing to enhanced precipitation over northern Congo. It is therefore anticipated that a better understanding of the linkages between upper-level winter troughs in these regions and tropical conditions to the south, including features relevant to operational forecasting like the ITD, may be expected to bring increased weather and sub-seasonal predictability to the tropical events, as well as building understanding and potential predictability on longer timescales (e.g., T18).

The goal of the present work is to deliver a more longitudinally-continuous knowledge on the low-latitude expression of troughs spanning 51.75° W–51.75° E. A specific aim is to provide a more complete presentation of troughs from Iberia to CM; W21 described how these troughs connected to low latitudes, but it was not clear whether the expression of troughs gradually evolved moving across these longitudes, or if Iberia and CM represented poles of high activity and impact. In addition, this new work aims to show how the signature of troughs evolves as the anchor longitude transitions westwards into the Atlantic, and eastwards into southwestern Asia. The focus is on low-level temperature, mid-level moisture and precipitation (building on W21 and T18), aiming to bring physical climate insights, but also perspectives relevant to operational forecasting of temperature and rainfall events.

Section 2 describes data and methods. Section 3 provides contextual analysis, presenting an overview of where and when in the annual cycle the strongest troughs occur and, using low-level temperature, establishing how the low-latitude signal of troughs evolves with time of year, specifically, moving out of mid-winter and into the transition seasons. Section 4 summarizes the December–March expression of troughs for various atmospheric parameters. Section 5 reinforces the relevance of the findings by quantifying the association of troughs with the large-scale northern Africa synoptic features of near-surface heat low and ITD. The concluding discussion (Section 6) includes consideration of the receptiveness at these longitudes, based on established linear theory, for Rossby wave propagation (e.g., Knippertz, 2007).

2 | DATA AND METHODS

Daily mean reanalysis fields are used from the European Centre for Medium-Range Weather Forecasts (ECMWF) product ERA5 (Hersbach et al., 2020), downloaded at 0.75° × 0.75° resolution over 1982–2020. In addition, the Multi-satellitE Retrievals for GPM (IMERG V6; Huffman et al., 2019) precipitation estimates were downloaded on the same grid for the period 2001–2019. Daily anomalies were calculated for each grid location, using a 31-day running mean climatology (W21). A separate analysis was made of the ERA5 10-m dew point temperature (at resolution of 0.25° × 0.25°) to diagnose the ITD.

To identify strong trough days at each longitude, a trough parameter (TP) index is calculated for a given 9.75° latitude zone (illustrated in Figures 1 and S1):

$$\mathrm{TP} = \left(\frac{Z_1 + Z_3}{2}\right) - Z_2, \tag{1}$$

where Z_2 is the average geopotential height anomaly at 200 hPa (Z200) for a 9.75° longitude zone centred on the target trough longitude, and Z_1 and Z_3 are average Z200 anomalies for the 12.0° zones to the west (Z_1) and east (Z_3)

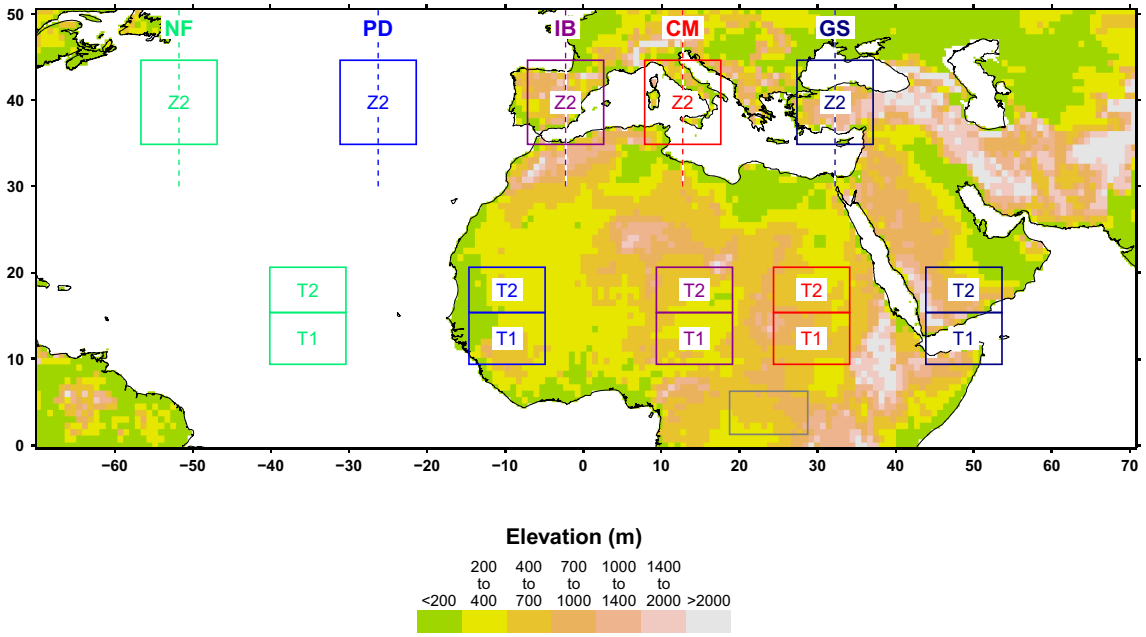

FIGURE 1 Some of the key trough locations and associated downstream domains used in the analyses, along with topographic elevation for reference. Target trough longitudes shown are: 51.75° W, shown in green and termed Newfoundland (NF); 26.25° W, blue, termed Ponta Delgado (PD); 2.25° W, magenta, termed Iberia (IB); 12.75° E, red, termed Central Mediterranean (CM); 32.25° E, dark blue, termed Gulf of Suez (GS). In each case, the box delimits the central Z2 domain (see Equation 1) used in the trough parameter calculation, while the vertical dashed line indicates the central longitude of Z2 (the target trough longitude). For each target trough longitude, T1 and T2 indicate key downstream domains used for indices: the domains are 9.75° longitude in width; T1 for grid-boxes centred 9.75–15° N (indices generally referred to as 10–15° N), T2 for grid-boxes centred 15.75–20.25° N (indices generally referred to as 15–20° N); the mid-points of T1 and T2 are 16.5° longitude downstream of the midpoint of Z2. Shading gives elevation over land. The grey box (1.25–6.25° N, 18.75–28.75° E) marks the northeastern Congo domain.

of Z_2. Large values of TP indicate the presence of a strong trough; explicitly, it measures the zonal gradient into the target (anchor) trough longitude (Knippertz, 2004), and may also be considered a finite difference measure of the curvature associated with the trough. In W21, the anchor latitude for the TP calculation was guided by the latitude (approximately 40° N) showing strongest Z200 linkage to northern Congo's daily rainfall. Tests (exploring TPs anchored from 33.75° N to 45.75° N at 1.5° increments) have shown the results highlighted here are robust when the anchor latitude is adjusted by a few degrees around 40° N (e.g., see Figure S2a,b), so for consistency, all results presented use 40° N. Similarly, the zonal scale of the TP calculation is mainly empirically informed (e.g., Jacobeit, 1987; Knippertz, 2004; W21). Future TP formulations may draw more explicitly on theoretical studies of the troughs and their linkages (e.g., Van der Wiel et al., 2015).

Mean composite anomaly fields for a range of variables are calculated for the strongest trough days. Results presented follow W21 in using the strongest 20% of days for the composite sample, and applying the same t-test approach to assess the statistical significance of the composite anomaly. The broad features emphasized here are not sensitive to the choice of sub-periods within 1982–2020, suggesting they are robust within the context of the more systematic long-term changes occurring over Africa at this time of year (T18; Hart et al., 2019; Hua et al., 2018). More specifically, the temperature results reported here are found to be especially consistent over time, while moisture features are generally of similar pattern but weaker in magnitude in the earlier years of ERA5.

3 | ANNUAL CYCLE OF STRONG TROUGH OCCURRENCE AND THE LOW-LATITUDE TEMPERATURE LINKAGE

Strong troughs, as measured by the TP applied to Z200 anomalies, are found to occur near 40° N in December–March across all longitudes in the analysis domain (Figure 2a), though these months do not represent a pronounced maximum in the annual cycle. June–September is however a distinct minimum. In mid-winter (most notably January), a modest reduction in frequency is found near the Azores High and for southwestern Asia

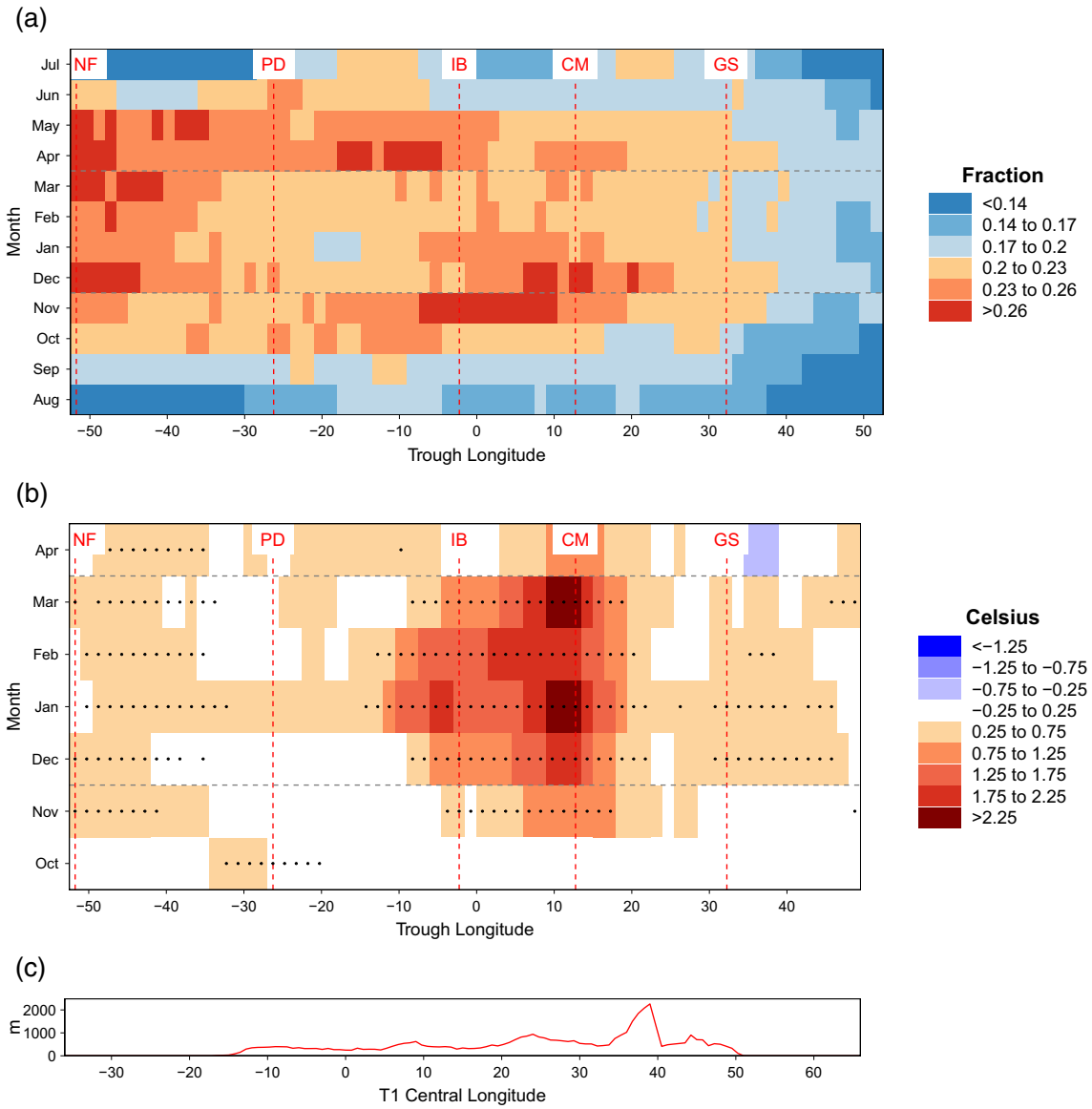

FIGURE 2 (a) Annual cycle of strong trough occurrence near 40° N (based on daily anomalies of 200-hPa geopotential height). The threshold to define a strong trough day is taken as the 20th percentile of trough parameter values over all longitudes and months (41.8 m), and the value plotted is the fraction of days above the threshold. The *x*-axis is the longitude used for the trough parameter and results are for 1982–2020. Vertical red dash lines indicate the trough longitudes highlighted on the location map (Figure 1). (b) Composite mean anomaly of 850-hPa temperature at 10–15° N following strong troughs (20% strongest during 1982–2020), shown here for Day +2. Strong troughs are identified separately for each climatological month, for example, for December, the sample is size 31 days × 39 years × 20% = 242 strong trough days (rounded to the nearest integer). The *x*-axis is the longitude used for the trough parameter. Geographic location of the anomaly shown is 16.5° longitude downstream (east) of the central trough axis (see T1 block average location examples in Figure 1). Black dots indicate that statistical significance (at the 1% level) is achieved by >90% of the 0.75° boxes making up the block average (T1 on Figure 1). To highlight the tendency in the 850-hPa temperature anomaly, values shown are relative to the average anomaly over Days −3 to −5. (c) Elevation averaged over 10–15° N. Note that the longitude axis is shifted 16.5° to the east relative to that used in (b), so the panel directly indicates the elevation found at the central longitude of the plotted 850-hPa temperature anomaly in (b).

(east of 40° E), although for both these zones, 14%–20% of days are still defined as strong trough days. When actual values of Z200 are used to define TP values, the pattern in Figure 2a is largely reproduced, but with longitude variations amplified, reflecting areas where climatological ridges and troughs tend to prevail. However, since the paper is primarily concerned with departures from the mean annual cycle, the results presented hereon continue to focus on TP values defined using Z200 anomalies. The results in Figure 2a are consistent with previous studies (e.g., Fröhlich & Knippertz, 2008; Matthiä, 2012) but adding monthly resolution to the previous trimester

season analyses, for example identifying November and April across the eastern Atlantic and Mediterranean as continuing and even increasing further upon the high frequency of occurrence in winter.

Having established that strong troughs can occur across all longitudes over the months October–April (Figure 2a), these troughs are now evaluated for the extent to which they deliver the low-latitude temperature signal found in W21. To provide this summary, Figure 2b shows the 850-hPa temperature (T850) anomaly at 10–15° N shifted by 16.5° longitude downstream (east) from the trough axis (Figure 1). This shift in longitude revealed the strongest response for Iberia and CM troughs in W21 and proves an efficient summary of the linkage here (results being insensitive to small changes in the shift). The response at Day +2 (Figure 2b) summarizes well the month and longitude variation of the signal. The response over Africa peaks at >2.5°C, about five times that found at other longitudes.

Over Africa, December–March is quite coherent, with November displaying a similar pattern but reduced magnitude, while October and April are substantially different. Considering other lags to Day +10 (not shown) does not alter this assessment, with the possible exception of March, which weakens after about lag Day +4 relative to December–February. The magnitude of the signal in Figure 2b peaks with troughs near CM, when the T850 box is clear of the Ethiopian Highlands (Figure 2c). For troughs east of CM, the T850 signal rapidly declines; this corresponds to a break-down of the signal as the Ethiopian Highlands are approached, and emerges overwhelmingly in Figure 2b,c.

A tendency for strongest trough occurrence (e.g., for November and April on Figure 2a) does not automatically translate into strongest T850 anomalies over Africa (Figure 2b). Also, in mid-winter (January–February), the main warming signature (Figure 2b) extends further westward to troughs in the eastern Atlantic (to about 15° W). Thus, future studies may address this mid-winter observation. However, for the bulk of the signal, Figure 2b supports pooling of December–March to generate efficient summaries, and this is applied in subsequent sections.

4 | DECEMBER–MARCH TROUGH EXPRESSION

When T850 is assessed near 15–20° N (as opposed to 10–15° N in the previous section), a more generic response is seen across all longitudes, at least for short lags out to Day +2/+3 (Figure 3a). In addition, there is now not a sharp break moving beyond CM, but rather a gradual damping of signal as trough impacts are now measured north of the Ethiopian Highlands, passing through eastern Sudan and across the Red Sea. Moving further east, troughs near the Gulf of Suez now project at these latitudes (i.e., 15–20° N) mostly to land over the Arabian Peninsula, and it is noticeable that response is now larger (box-average peaking around 1.75°C), though this is still substantially less than found over central Africa (which peaks about twice as large). In addition, Figure 3a reveals the length of persistence of the warming signal is unique to Africa, growing especially strong around Iberia troughs, with statistical significance extending out to Day +10. Indeed, for troughs east of CM extending to southwestern Asia, there is a tendency for the warm anomalies to be replaced by significant cold anomalies over Days +5 to +10, likely reflecting cold advection as the trough moves eastward.

Further uniqueness in the T850 warm signature over Africa emerges for larger geographic shifts. For the latitude band 10–15° N, Figure 3b measures T850 at a shift that is equivalent to moving from Iberia to northeastern Congo (a shift of 26.25° longitude, see Figure S1c). It reveals unique magnitude, significance and persistence (up to 10 days) over Africa, with minor areas of low-amplitude response and significance near Newfoundland and Gulf of Suez. Over Africa, the signal peaks for troughs at 5.25° E (T850 measured at box centred 31.5° E); it then decays for troughs further east as the T850 box extends into the Ethiopian Highlands. When T850 is measured at 15–20° N (not shown), the response over Arabia is amplified, but not as clearly as in Figure 3b. The implication is that a 16.5° shift (Figure 3a) appears to represent a natural spatial scale for the troughs, but responses at larger shifts require the unique geographic and dynamic setting of Africa (Figure 3b).

The trough linkage to near-equatorial northern Congo precipitation (W21) is found to be present for all troughs from west of Iberia to the east of CM (at the preferred 16.5° shift), while no other trough longitudes display such precipitation enhancement (Figure 3c). Near 10° W, the anomaly actually switches sign, with negative precipitation anomalies continuing clearly to about 25° W; the longitude shift means this response is mostly over the ocean in the Gulf of Guinea (5° E–10° W), and the notion of a north–south dipole, with moisture enhanced to the north over West Africa land, is returned to in Section 5.

The negative precipitation anomalies for troughs east of CM (troughs at 17.25–21.75° E, Figure 3c) resemble a geographic squeeze on the preferred trough expression, with positive anomalies occurring at shorter shifts (not shown), while the 16.5° shift for these troughs enters the Rift Valley Highlands, moving beyond the approximate

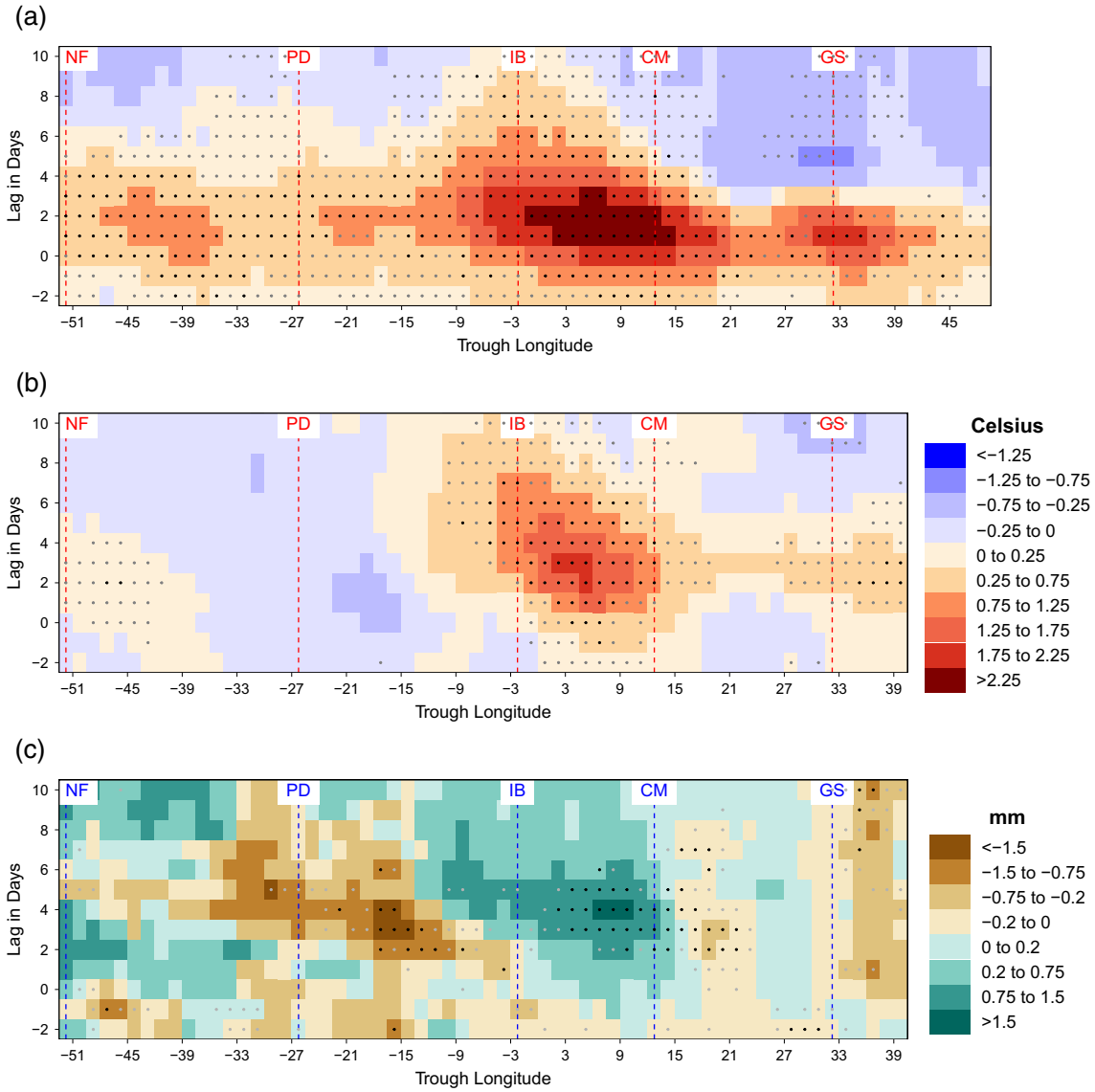

FIGURE 3 (a) Composite mean anomaly of 850-hPa temperature at 15–20° N for lags relative to strong trough days (20% strongest during 1982–2020). All results are calculated individually for each month December–March, and the four composite fields averaged to provide a summary for December–March. Geographic location of the anomaly shown is 16.5° longitude downstream of the central trough axis (see T2 block average location examples in Figure 1). Black dots indicate that statistical significance (at the 1% level) is achieved by >90% of the 0.75° boxes making up the block average in at least 3 of the 4 constituent months; light grey dot indicates at least 1 of the constituent months. To highlight the tendency in the 850-hPa temperature anomaly, values shown are relative to the average anomaly over Days −3 to −5. (b) Same as (a) but for 10–15° N and shift of 26.25° longitude. (c) Same as (a) but for precipitation averaged for grid-boxes centred 1.5–6.0° N (indices generally referred to as 1–6° N), and analysis period of 2001–2019. Grid-box precipitation is noisy; to give some impression of where the results are above the noise level, black dots indicate that statistical significance (at the 20% level) is achieved by >40% of the 0.75° boxes making up the block average in at least 3 of the 4 constituent months; light grey dot indicates at least 2 of the constituent months. Results with outgoing longwave radiation achieve much clearer statistical significance due to the naturally less-noisy field (W21), but precipitation is shown here given its direct weather relevance.

30° E boundary that marked an east–west dipole of moisture response in W21 (and seen elsewhere, e.g., Jackson et al., 2019; Finney et al., 2020). These results (and others highlighted in the paper) are found to be robust for moderate changes in the target trough latitude: for example, Figure S2a,b reveals insensitivity to moving the TP calculation southwards. However, precipitation results are clearly sensitive to composite latitude band (compare Figure S2c with Figure 3c).

While the near-equatorial enhanced precipitation signal is found to be uniquely strong for northern Congo longitudes (Figure 3c), the mid-level moisture signature

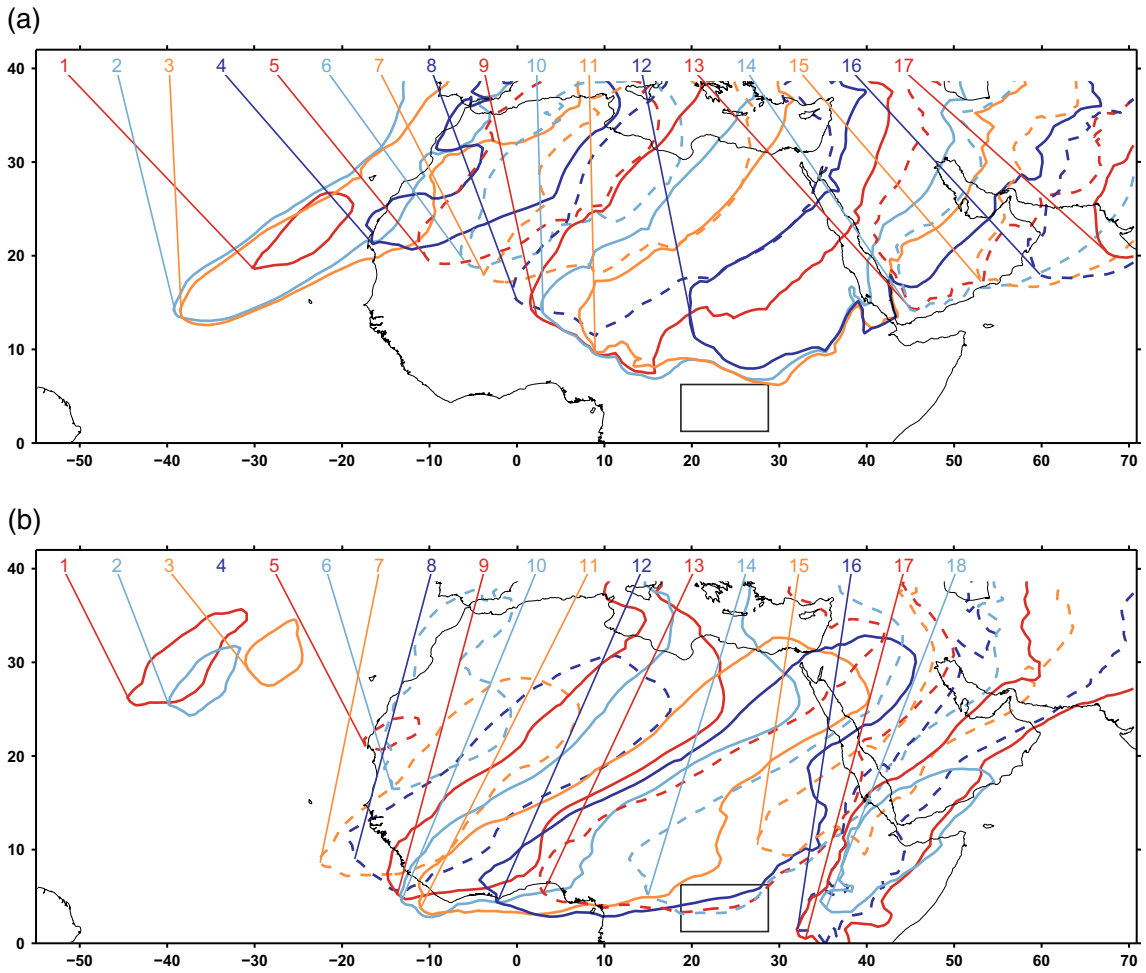

FIGURE 4 (a) Composite mean anomaly of 850-hPa temperature 3 days after the strong trough days (20% strongest during 1982–2020) for selected trough longitudes (labelled 1–17). The +1°C anomaly contour is plotted for each trough, with a solid line connecting the trough anchor location (the central latitude and longitude of the trough parameter) to the southwesternmost point on the associated contour. Troughs shown are at 6° longitude intervals starting at 51.75° W and extending to 44.25° E (Trough 18 at 50.25° E was analysed, but is not shown since the +1°C contour is outside the analysis domain). The first panel is for all troughs, followed by animation sequence showing each trough individually from west to east. Colours and solid/dashed line style are used to help more clearly view each contour. (b) Same as (a) but for 600-hPa specific humidity 1 day after the strong trough, showing the +0.2 $g \cdot kg^{-1}$ anomaly contour (except Trough 4, which has no such contour). For both (a) and (b), only the main contour to the south and east of the trough is plotted for clarity. For reference, the grey box is northeastern Congo.

(600-hPa specific humidity [Q600]) presented in W21 turns out to have expression for all troughs from the eastern Atlantic to southwestern Asia (Figure S3). The T850 and Q600 signatures are spatially mapped in Figure 4, based on a subset of the TP indices (Table S1) and highlighting Day +3 for T850 and Day +1 for Q600. A systematic T850 pattern and systematic Q600 pattern emerges, with spatial variations as a function of longitude likely reflecting local geographic and background climatic settings shaping the exact expression at each longitude, such as in relation to the Ethiopian Highlands, with the contrasting T850 expression of Troughs 12 and 13. The following summary begins with the troughs that project strongly into central Africa (as in W21). The summary then describes how this signature transforms as trough anchor longitudes transition westward (ii-iii below) and eastward (iv-v below).

i. Troughs 9–12: these troughs, extending from just west of Iberia to the east of CM, reflect the strong signature reported in W21. The +1°C anomaly contour extends south of 10° N for these troughs, close to northern Congo, while positive Q600 anomalies stream from near 5° N in the Gulf of Guinea northeastward, extending close to northern Congo, especially for Troughs 11 and 12. Overall, these troughs yield a unique juxtaposition of T850 and Q600 anomalies at near-equatorial latitudes.

ii. Troughs 4–8: these troughs anchored in the easternmost Atlantic are transitional, with some elements of (i) present. Troughs 7 and 8 are the westernmost troughs to display substantial Q600 signature. They also display T850 signature southward to 15° N and do impact near-surface features extending into the deep tropics of West Africa (see Section 5). Troughs 4–6 have a moderate T850 signal but it does not persist (Figure 3a) or spread (Figure 3b). Trough 4 is the first trough with T850 impacts to cross the Atlas Mountains.

iii. Troughs 1–3: impacts of these troughs remain over the Atlantic Ocean, with T850 expression locked west of the Atlas Mountains and Q600 signature remaining local to the trough.

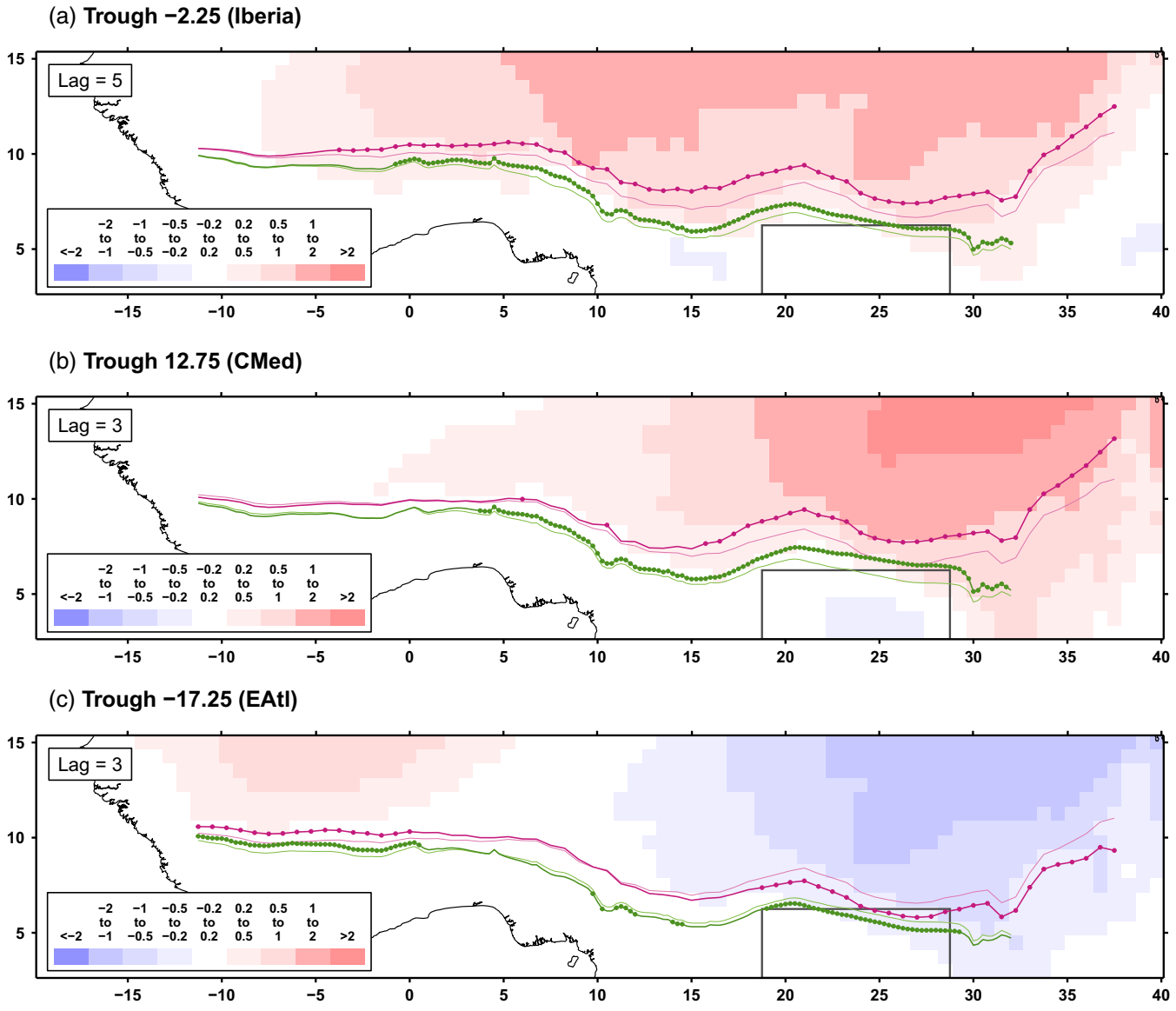

FIGURE 5 (a) Composite mean of the intertropical discontinuity and heat low latitudes along with 850-hPa temperature anomalies, for strong Iberia (2.25° W) troughs (20% strongest 1982–2020). All results are calculated individually for each month December–March, and the four composite fields/latitudes are averaged to provide a summary for December–March. The first panel is for Day +5 (when features are close to maximum development) followed by daily animation sequence from Day −5 to Day +10. Thick pink line is the composite mean latitude of the heat low (thin pink line is the climatological latitude); thick green line is the composite mean latitude of the intertropical discontinuity (thin green line is the climatological latitude). Bold dots indicate where at least 3 of the 4 constituent months showed a significant displacement of latitude at the 5% level. (b) Same as (a) but for troughs at 12.75° E (central Mediterranean), and first panel for Day +3. (c) Same as (a) but for troughs at 17.25° W (eastern Atlantic), and first panel for Day +3. The grey box is northeastern Congo.

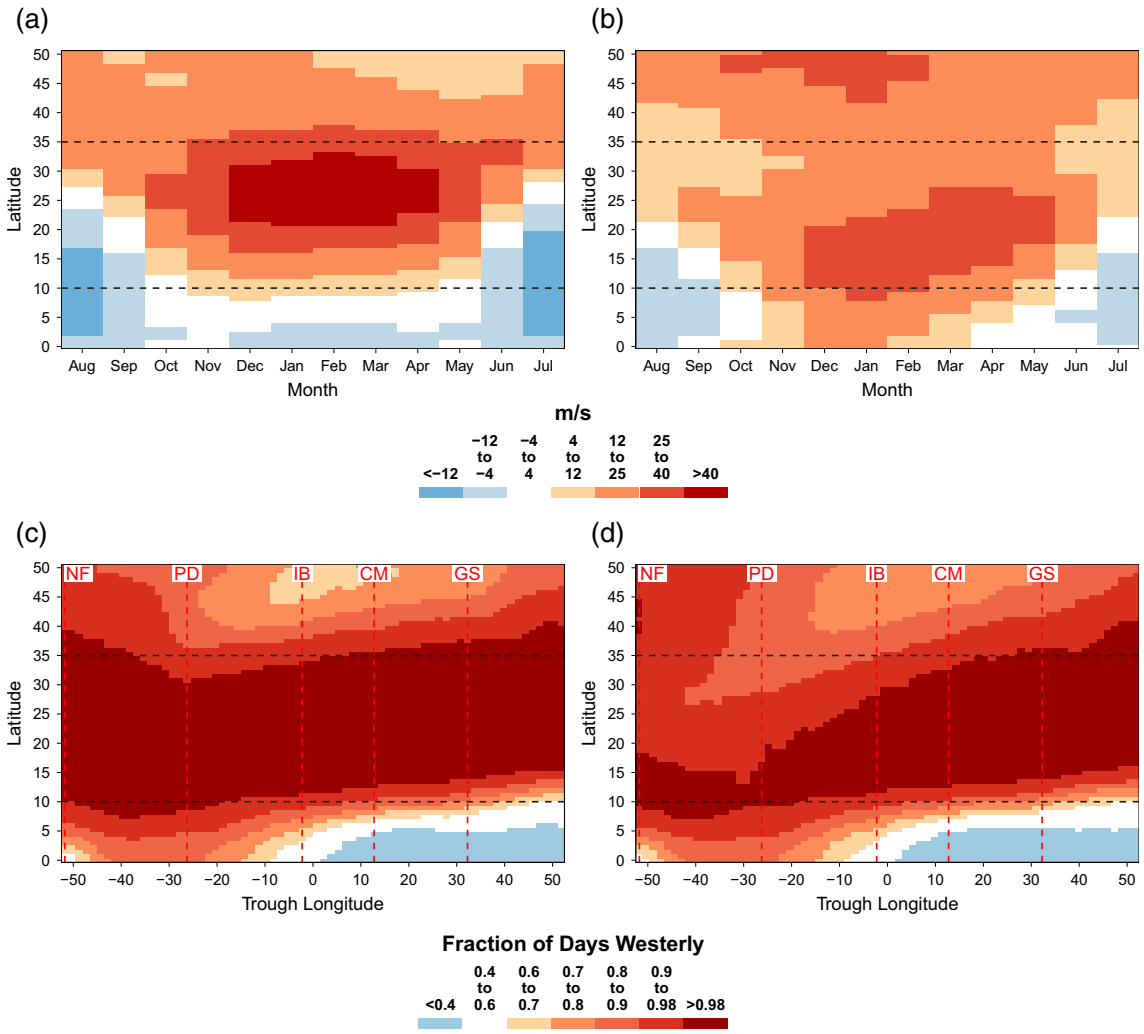

FIGURE 6 (a) Climatology (1982–2016) of 200-hPa zonal wind averaged over the 9.75° longitude block centred on 24° E (i.e., the approximate longitudes of northeastern Congo). (b) Same as (a) but centred on 30° W (central Atlantic). (c) For the 20% of strongest trough days (as identified at each longitude), the shading indicates the fraction of December–March days (1982–2020) with westerly wind at 200-hPa (based on 9.75° longitude average blocks centred on the trough longitude). (d) Same as (c) but for 2 days after the strongest trough days.

iv. Troughs 13–14: the Q600 signature extends from equatorial latitudes like in group (i), but the T850 signature has now migrated eastward beyond the Ethiopian Highlands and now begins over the Arabian Peninsula. The signature in Q600 resembles that shown to impact weather anomalies to the northeast, such as extreme precipitation events in the Levant and Saudi Arabia (e.g., De Vries et al., 2016; Ziv, 2001).
v. Troughs 15–18: the T850 expression of these troughs is now mostly east of the Arabian Peninsula extending to border regions of South Asia. Particularly, Troughs 16 and 17 develop a Q600 signature extending from equatorial eastern Africa to southwestern Asia, bordering into South Asia.

Strong troughs at these latitudes are inherently associated with upper-level potential vorticity (PV) anomalies (illustrated for the composite means here in Figure S4). Further work is needed to assess if troughs with particularly strong, vertically deep and meridionally perturbed PV signatures have an amplified impact (e.g., will the fields in Figure 4 become even stronger?). This possibility is suggested by case studies of troughs over the eastern Atlantic approaching the western Mediterranean (e.g., Knippertz, 2007; Knippertz & Martin, 2005) where a PV framework (i) provided insights into upstream ridge developments that could initiate the equatorial portion of the TPs, and (ii) showed how strong PV anomalies extending southward associated with the trough itself can more directly enhance rainfall events (e.g., Fink & Knippertz, 2003); such PV anomalies have also been directly related to rainfall events over the Arabian Peninsula (De Vries et al., 2018) and other regions including the Australian monsoon (Berry et al., 2012).

5 | ITD AND HEAT LOW

The ITD and, in the hot dry air to its north, the low-level heat low (HL), represent key features in the functioning of weather and climate variability across tropical northern Africa (e.g., Cornforth et al., 2017; Fink et al., 2011; Knippertz & Fink, 2008; Lavaysse et al., 2009; Nicholson et al., 2021). Connecting the T850 and other aspects of the trough composites (e.g., Figures 2b and 4) to fluctuations in these synoptic features would reinforce the relevance of findings to operational meteorology as well as advancing understanding of the trough impacts. To make such assessment, daily analysis of the ITD latitude (latitude of the 14°C dew point temperature) and latitude of strongest HL expression (latitude of the maximum 925- to 600-hPa thickness) has been undertaken (these approaches building on established methods in the above references; see Figure S5 for description of how each day's latitude is estimated here). For the strong trough days, composites of the mean latitude of these features have been calculated across northern Africa. These are graphically compared to the climatological latitude (Figure 5), while statistical significance is estimated using the daily anomalous latitude departures (*t*-test, see Section 2).

For Iberia troughs (Figure 5a) and CM troughs (Figure 5b) statistically significant northward departures in ITD and HL (peaking about 1.5° latitude shift near northeastern Congo in the composite mean) are found tracking the longitude of T850 anomalies, whose centre of axis migrates eastward in the days after the strong trough. For Iberia, the T850 anomalies, accompanied by HL and ITD, move a greater distance and more slowly west-to-east (consistent with the larger migration and slower timescale proposed for Iberia impacts in W21). The impression is gained on occasions that the T850 anomalies and HL departures precede slightly the ITD departures (for future investigation). For troughs at 5.25° E, perturbation of the ITD and HL (Figure S5a) is again strong, with timing in between Iberia and CM (Figure 5a,b).

Troughs in the easternmost Atlantic are associated with moderate low-level warming and northward shift of the ITD and HL in West Africa (Figure 5c, trough at 17.25° W), reinforcing previous dry-season case studies and assessments in this region (Knippertz & Fink, 2008; Nicholson, 1981). The suggestion is that troughs accompany a northward shift in moisture from the Gulf of Guinea (the negative precipitation anomalies in Figure 3c) into West Africa over these longitudes. Troughs to the east of CM are distinct in gradually developing a cooling signature at low latitudes over Africa (even downstream from the original trough, Figure 3a), and this is clearly seen in Figure S5b (trough at 27.75° E) with ITD and HL strongly displaced southward by Day +3, consistent with Vizy and Cook (2014).

6 | CONCLUDING DISCUSSION

This paper has analysed midlatitude upper-level troughs across the 51.75° W-51.75° E sector, and revealed their amplified low-latitude expression over northern Africa, with implications for operational weather forecasting. This is especially the case for most northeastern parts, where downstream low-level warming following the troughs extends south of 10° N, close to a tropical plume of mid-level moisture. The main Congo rain belt extends further north, and the ITD and HL migrate north. West Africa experiences a similar response (Knippertz & Fink, 2008), though less in magnitude. Moving east, the Arabian Peninsula experiences a substantial warming following troughs, but much shorter (2–3 days, compared to up to 10 for northern Africa), and typically not with the same geographic relation to the mid-level moisture plume, which has been shown of itself to impact extreme rain events (De Vries et al., 2016; Ziv, 2001). Over the central Atlantic, troughs do also lead to a small low-level warming for a few days near 15–20° N, the implications of which, including for ocean–atmosphere developments, require further investigation.

The strong troughs studied here may often be related to Rossby waves propagating on the nearby midlatitude and subtropical waveguides (e.g., Röthlisberger et al., 2016). Early work identified the coupling of the Mediterranean and Central Africa as a candidate for tropical–extratropical interaction related to Rossby wave propagation, based on empirical analysis (point correlation, Kiladis & Weickmann, 1992) and theoretical modelling (linear Rossby waves, Hoskins & Ambrizzi, 1993). Indeed, the upper-level winter zonal wind climatology, in terms of linear Rossby wave theory (Held et al., 2002; Yang & Hoskins, 1996), is well suited to wave propagation over the subtropical latitudes of Africa into the tropics (Figure 6a) until the critical latitude will typically be approached near 5–10° N as strong westerly winds transition rapidly to easterly (there is no critical latitude in winter over the central Atlantic, Figure 6b). Situations with some commonalities have now been widely studied in many regions including South America and the nearby Atlantic, Australia and the nearby western Pacific and the North American monsoon (Berry & Reeder, 2016; Pascale et al., 2016; Van der Wiel et al., 2015; Zilli & Hart, 2021). Various aspects emerge in these works, including refraction of Rossby waves equatorward, meridional expansion of Rossby waves as jet exits are approached leading to equatorward engagement

including frontal development as a possible factor in establishing warm and moist air ahead of the trough (Berry & Reeder, 2016), the breaking of Rossby waves and entrainment of PV anomalies equatorward (Berry et al., 2012) and the impact on synoptic systems of variations in critical latitude (Zilli & Hart, 2021). Such assessments will likely yield insights to the mechanisms associated with the synoptic developments presented here over northern Africa. During the strong troughs over Africa longitudes, zonal wind south of the trough actually further increases its tendency to be westerly and becomes substantially stronger in the mean (Figures 6c,d and S6a). This may pose a challenge for detailed assessment, since established linear Rossby wave theory assumes a stationary background flow, whereas the eddies here represent a substantial perturbation to the mean state. In terms of the critical latitude itself, while it does not appear to shift substantially in the mean composite, there is nonetheless a sharpening of the transition to easterlies over Africa in the days following the strong troughs (Figure S6b, consistent with Kiladis & Weickmann, 1992).

Further work could consider optimizing some methodological aspects of this study, such as the latitude used to detect the troughs and the location of downstream indices. Nonetheless, the details presented here can help guide the investigation of the physical processes giving rise to the mode of variation over Africa, including the ITD/near-equatorial moisture signatures and the near-surface temperature anomalies. The longitudinally varying development of the latter may at least in part be linked to contrasts in the gradient of the temperature anomaly fields themselves (e.g., Figure 4a) combined with circulation, given previous regional perspectives on advection (Hu et al., 2019; Vizy & Cook, 2014). Finally, T18 and W21 started to look at the climate variations in the region and relate these to the synoptic timescale trough impacts (including some features extending south of the equator); the continuous longitude perspective developed here can now inform the efficient development of such climate timescale work.

AUTHOR CONTRIBUTIONS

Neil Ward: Writing – original draft. **Andreas H. Fink:** Writing – review and editing. **Richard J. Keane:** Writing – review and editing. **Douglas J. Parker:** Writing – review and editing.

ACKNOWLEDGEMENTS

Douglas J. Parker was supported by AMMA-2050 (NERC/DFID NE/M020126/1), IMPALA (NERC/DFID NE/M017176/1) and by the UK Research and Innovation as part of the Global Challenges Research Fund, African SWIFT programme, grant number NE/P021077/1; Richard J. Keane has been supported by CEMAC, University of Leeds. Andreas H. Fink acknowledges support from the Transregional Collaborative Research Center SFB/TRR 165 'Waves to Weather' (www.wavestoweather.de) funded by the German Research Foundation (DFG). The authors are grateful for the insightful comments of the two reviewers, which led to substantial manuscript improvements. The authors are grateful to the data providers (ERA5 provided by Copernicus Data Store through https://www.ecmwf.int/en/forecasts/datasets/reanalysis-datasets/era5; IMERG provided by NASA https://disc.gsfc.nasa.gov/; topographic information for Figure 1 built from http://research.jisao.washington.edu/data_sets/elevation/; drawing on for land/water designation: 0.25° interpolated from TerrainBase, Global 5 Arc-minute Ocean Depth and Land Elevation, DOI: 10.5065/E08M-4482 and for elevation: 0.75° ERA grid interpolated from ETOPO5 Global Earth Topography, 5-min, DOI: 10.5065/D62F7KG0).

ORCID

Neil Ward https://orcid.org/0000-0003-1385-0349
Andreas H. Fink https://orcid.org/0000-0002-5840-2120

REFERENCES

Bekele-Biratu, E., Thiaw, W.M. & Korecha, D. (2018) Sub-seasonal variability of the Belg rains in Ethiopia. *International Journal of Climatology*, 38(7), 2940–2953. https://doi.org/10.1002/joc.5474

Berry, G.J. & Reeder, M.J. (2016) The dynamics of Australian monsoon bursts. *Journal of the Atmospheric Sciences*, 73(1), 55–69. https://doi.org/10.1175/JAS-D-15-0071.1

Berry, G.J., Reeder, M.J. & Jakob, C. (2012) Coherent synoptic disturbances in the Australian monsoon. *Journal of Climate*, 25(24), 8409–8421. https://doi.org/10.1175/JCLI-D-12-00143.1

Camberlin, P. & Philippon, N. (2002) The East African March–May rainy season: associated atmospheric dynamics and predictability over the 1968–97 period. *Journal of Climate*, 15(9), 1002–1019. https://doi.org/10.1175/1520-0442(2002)015%3C1002:TEAMMR%3E2.0.CO;2

Cook, K.H. & Vizy, E.K. (2015) Detection and analysis of an amplified warming of the Sahara Desert. *Journal of Climate*, 28(16), 6560–6580. https://doi.org/10.1175/JCLI-D-14-00230.1

Cornforth, R., Mumba, Z., Parker, D.J., Berry, G., Chapelon, N., Diakaria, K. et al. (2017) Synoptic systems. In: Parker, D.J. & Diop-Kane, M. (Eds.) *Meteorology of tropical West Africa: the forecasters' handbook*. Hoboken, NJ: Wiley, pp. 40–89. https://doi.org/10.1002/9781118391297.ch2

De Vries, A., Feldstein, S.B., Riemer, M., Tyrlis, E., Sprenger, M., Baumgart, M. et al. (2016) Dynamics of tropical–extratropical interactions and extreme precipitation events in Saudi Arabia in autumn, winter and spring. *Quarterly Journal of the Royal Meteorological Society*, 142(697), 1862–1880. https://doi.org/10.1002/qj.2781

De Vries, A.J., Ouwersloot, H.G., Feldstein, S.B., Riemer, M., El Kenawy, A.M., McCabe, M.F. et al. (2018) Identification of

tropical-extratropical interactions and extreme precipitation events in the Middle East based on potential vorticity and moisture transport. *Journal of Geophysical Research: Atmospheres*, 123(2), 861–881. https://doi.org/10.1002/2017JD027587

Fink, A.H., Agustí-Panareda, A., Parker, D.J., Lafore, J.P., Ngamini, J.B., Afiesimama, E. et al. (2011) Operational meteorology in West Africa: observational networks, weather analysis and forecasting. *Atmospheric Science Letters*, 12(1), 135–141. https://doi.org/10.1002/asl.324

Fink, A.H. & Knippertz, P. (2003) An extreme precipitation event in southern Morocco in spring 2002 and some hydrological implications. *Weather*, 58(10), 377–387. https://doi.org/10.1256/wea.256.02

Finney, D.L., Marsham, J.H., Walker, D.P., Birch, C.E., Woodhams, B.J., Jackson, L.S. et al. (2020) The effect of westerlies on East African rainfall and the associated role of tropical cyclones and the Madden–Julian Oscillation. *Quarterly Journal of the Royal Meteorological Society*, 146(727), 647–664. https://doi.org/10.1002/qj.3698

Fröhlich, L. & Knippertz, P. (2008) Identification and global climatology of upper-level troughs at low latitudes. *Meteorologische Zeitschrift*, 17, 565–573. https://doi.org/10.1127/0941-2948/2008/0320

Fröhlich, L., Knippertz, P., Fink, A.H. & Hohberger, E. (2013) An objective climatology of tropical plumes. *Journal of Climate*, 26(14), 5044–5060. https://doi.org/10.1175/JCLI-D-12-00351.1

Hart, N.C., Washington, R. & Maidment, R.I. (2019) Deep convection over Africa: annual cycle, ENSO, and trends in the hotspots. *Journal of Climate*, 32(24), 8791–8811. https://doi.org/10.1175/JCLI-D-19-0274.1

Held, I.M., Ting, M. & Wang, H. (2002) Northern winter stationary waves: theory and modeling. *Journal of Climate*, 15(16), 2125–2144. https://doi.org/10.1175/1520-0442(2002)015%3C2125:NWSWTA%3E2.0.CO;2

Hersbach, H., Bell, B., Berrisford, P., Hirahara, S., Horányi, A., Muñoz-Sabater, J. et al. (2020) The ERA5 global reanalysis. *Quarterly Journal of the Royal Meteorological Society.*, 146, 1999–2049. https://doi.org/10.1002/qj.3803

Hoskins, B.J. & Ambrizzi, T. (1993) Rossby wave propagation on a realistic longitudinally varying flow. *Journal of Atmospheric Sciences*, 50(12), 1661–1671. https://doi.org/10.1175/1520-0469(1993)050%3C1661:RWPOAR%3E2.0.CO;2

Hu, L., Luo, J.-J., Huang, G. & Wheeler, M.C. (2019) Synoptic features responsible for heat waves in Central Africa, a region with strong multidecadal trends. *Journal of Climate*, 32(22), 7951–7970. https://doi.org/10.1175/JCLI-D-18-0807.1

Hua, W., Zhou, L., Chen, H., Nicholson, S.E., Jiang, Y. & Raghavendra, A. (2018) Understanding the central equatorial African long-term drought using AMIP-type simulations. *Climate Dynamics*, 50(3–4), 1115–1128. https://doi.org/10.1007/s00382-017-3665-2

Huffman, G.J., Stocker, E.F., Bolvin, D.T., Nelkin, E.J. & Tan, J. (2019) *GPM IMERG final precipitation L3 1 day 0.1 degree x 0.1 degree V06*. Savtchenko, A. (Ed.) Greenbelt, MD: Goddard Earth Sciences Data and Information Services Center (GES DISC). https://doi.org/10.5067/GPM/IMERGDF/DAY/06

Jackson, L.S., Keane, R.J., Finney, D.L., Marsham, J.H., Parker, D.J., Senior, C.A. et al. (2019) Regional differences in the response of rainfall to convectively coupled kelvin waves over tropical Africa. *Journal of Climate*, 32(23), 8143–8165. https://doi.org/10.1175/JCLI-D-19-0014.1

Jacobeit, J. (1987) Variations of trough positions and precipitation patterns in the Mediterranean area. *Journal of Climatology*, 7(5), 453–476. https://doi.org/10.1002/joc.3370070503

Kiladis, G.N. & Weickmann, K.M. (1992) Circulation anomalies associated with tropical convection during northern winter. *Monthly Weather Review*, 120(9), 1900–1923. https://doi.org/10.1175/1520-0493(1992)120%3C1900:CAAWTC%3E2.0.CO;2

Knippertz, P. (2004) A simple identification scheme for upper-level troughs and its application to winter precipitation variability in Northwest Africa. *Journal of Climate*, 17(6), 1411–1418. https://doi.org/10.1175/1520-0442(2004)017%3C1411:ASISFU%3E2.0.CO;2

Knippertz, P. (2007) Tropical–extratropical interactions related to upper-level troughs at low latitudes. *Dynamics of Atmospheres and Oceans*, 43(1–2), 36–62. https://doi.org/10.1016/j.dynatmoce.2006.06.003

Knippertz, P. & Fink, A.H. (2008) Dry-season precipitation in tropical West Africa and its relation to forcing from the extratropics. *Monthly Weather Review*, 136(9), 3579–3596. https://doi.org/10.1175/2008MWR2295.1

Knippertz, P. & Martin, J.E. (2005) Tropical plumes and extreme precipitation in subtropical and tropical West Africa. *Quarterly Journal of the Royal Meteorological Society*, 131(610), 2337–2365. https://doi.org/10.1256/qj.04.148

Lavaysse, C., Flamant, C., Janicot, S., Parker, D., Lafore, J.-P., Sultan, B. et al. (2009) Seasonal evolution of the West African heat low: a climatological perspective. *Climate Dynamics*, 33(2–3), 313–330. https://doi.org/10.1007/s00382-009-0553-4

Matthiä, S. (2012). Höhentröge und Niederschlagsstatistik in Nordwest-Afrika zwischen 1979 und 2011 (Master's thesis), Universität zu Köln, Cologne, Germany.

Nicholson, S.E. (1981) Rainfall and atmospheric circulation during drought periods and wetter years in West Africa. *Monthly Weather Review*, 109(10), 2191–2208. https://doi.org/10.1175/1520-0493(1981)109%3C2191:RAACDD%3E2.0.CO;2

Nicholson, S.E., Fink, A.H., Funk, C., Klotter, D.A. & Satheesh, A.R. (2021) Meteorological causes of the catastrophic rains of October/November 2019 in equatorial Africa. *Global and Planetary Change*, 208, 103687. https://doi.org/10.1016/j.gloplacha.2021.103687

Pascale, S., Bordoni, S., Kapnick, S.B., Vecchi, G.A., Jia, L., Delworth, T.L. et al. (2016) The impact of horizontal resolution on north American monsoon Gulf of California moisture surges in a suite of coupled global climate models. *Journal of Climate*, 29(21), 7911–7936. https://doi.org/10.1175/JCLI-D-16-0199.1

Röthlisberger, M., Martius, O. & Wernli, H. (2016) An algorithm for identifying the initiation of synoptic-scale Rossby waves on potential vorticity waveguides. *Quarterly Journal of the Royal Meteorological Society*, 142(695), 889–900. https://doi.org/10.1002/qj.2690

Taylor, C.M., Fink, A.H., Klein, C., Parker, D.J., Guichard, F., Harris, P.P. et al. (2018) Earlier seasonal onset of intense mesoscale convective systems in The Congo Basin since 1999. *Geophysical Research Letters*, 45(24), 13,458–13,467. https://doi.org/10.1029/2018GL080516

Van der Wiel, K., Matthews, A.J., Stevens, D.P. & Joshi, M.M. (2015) A dynamical framework for the origin of the diagonal South Pacific and South Atlantic convergence zones. *Quarterly*

Journal of the Royal Meteorological Society, 141(691), 1997–2010. https://doi.org/10.1002/qj.2508

Vizy, E.K. & Cook, K.H. (2014) Impact of cold air surges on rainfall variability in the Sahel and wet African tropics: a multi-scale analysis. *Climate Dynamics*, 43(3–4), 1057–1081. https://doi.org/10.1007/s00382-013-1953-z

Ward, N., Fink, A.H., Keane, R.J., Guichard, F., Marsham, J.H., Parker, D.J. & Taylor, C.M. (2021) Synoptic timescale linkage between midlatitude winter troughs Sahara temperature patterns and northern Congo rainfall: a building block of regional climate variability. *International Journal of Climatology*, 41(5), 3153–3173. https://doi.org/10.1002/joc.7011

Yang, G.-Y. & Hoskins, B.J. (1996) Propagation of Rossby waves of nonzero frequency. *Journal of Atmospheric Sciences*, 53(16), 2365–2378. https://doi.org/10.1175/1520-0469(1996)053%3C2365:PORWON%3E2.0.CO;2

Zilli, M.T. & Hart, N.C.G. (2021) Rossby wave dynamics over South America explored with automatic tropical–extratropical cloud band identification framework. *Journal of Climate*, 34(20), 8125–8144. https://doi.org/10.1175/JCLI-D-21-0020.1

Ziv, B. (2001) A subtropical rainstorm associated with a tropical plume over Africa and the Middle-East. *Theoretical and Applied Climatology*, 69(1), 91–102. https://doi.org/10.1007/s007040170037

SUPPORTING INFORMATION

Additional supporting information can be found online in the Supporting Information section at the end of this article.

How to cite this article: Ward, N., Fink, A. H., Keane, R. J., & Parker, D. J. (2023). Upper-level midlatitude troughs in boreal winter have an amplified low-latitude linkage over Africa. *Atmospheric Science Letters*, *24*(1), e1129. https://doi.org/10.1002/asl.1129